An experimental investigation into the partition of Mo between aqueous fluids and felsic melts: Implications for the genesis of porphyry Mo ore deposits

Ziqi Jiang, Linbo Shang, Haihao Guo, Xin-Song Wang, Chen Chen, Yunhe Zhou

Journal Pre-proofs

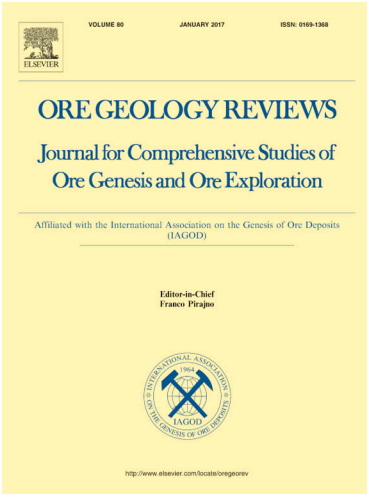

An experimental investigation into the partition of Mo between aqueous fluids and felsic melts: Implications for the genesis of porphyry Mo ore deposits

Ziqi Jiang, Linbo Shang, Haihao Guo, Xin-song Wang, Chen Chen, Yunhe Zhou

PII: S0169-1368(21)00169-4
DOI: https://doi.org/10.1016/j.oregeorev.2021.104144
Reference: OREGEO 104144

To appear in: *Ore Geology Reviews*

Received Date: 20 June 2020
Revised Date: 18 March 2021
Accepted Date: 20 March 2021

Please cite this article as: Z. Jiang, L. Shang, H. Guo, X-s. Wang, C. Chen, Y. Zhou, An experimental investigation into the partition of Mo between aqueous fluids and felsic melts: Implications for the genesis of porphyry Mo ore deposits, *Ore Geology Reviews* (2021), doi: https://doi.org/10.1016/j.oregeorev.2021.104144

An experimental investigation into the partition of Mo between aqueous fluids and felsic melts: Implications for the genesis of porphyry Mo ore deposits

Ziqi Jiang[a,b], Linbo Shang[a*], Haihao Guo[c], Xin-song Wang[a], Chen Chen[a,b], Yunhe Zhou[a,b]

[a] State Key Laboratory of Ore Deposit Geochemistry, Institute of Geochemistry, Chinese Academy of Sciences, Guiyang 550081, China

[b] University of Chinese Academy of Sciences, Beijing 100049, China

[c] ISTO, UMR 7327 CNRS-Université d'Orléans-BRGM, 45071 Orléans, France

Abstract

Most of the world's large molybdenum (Mo) deposits are genetically related to magmas that underwent significant fractional crystallization and fluid exsolution, and the residual silicate melts are commonly peralkaline. To understand the relationship between melt compositions and the genesis of porphyry Mo mineralization, the partition coefficients of molybdenum (D_{Mo}) between fluid and felsic melt were determined at 850 °C, 900 °C, and 100 MPa with various values of A/NK [molar Al_2O_3/ ($Na_2O + K_2O$) in the melt] under an oxygen fugacity around the Ni–NiO (NNO) buffer. The results show that D_{Mo} decreases from 4.23 to 0.4 with increasing A/NK from 0.75 to 1.36 in the carbon dioxide series (fluid composed of X_{CO_2}= 0.096 [molar CO_2/ (CO_2

+ H_2O)] and 17.5 wt.% NaCl). A similar trend was observed in pure water, with A/NK varying from 0.72 to 1.23, D_{Mo} decreases from 0.54 to 0.15. Significantly, D_{Mo} in peralkaline melt is consistently higher than that in peraluminous melt, even with the same NBO/T (the ratio of non-bridge oxygen and tetrahedron ion). Our study therefore reveals that Mo is easily distributed into fluids that exsolved from peralkaline magmas. This finding explains why highly fractionated magmas are critical for porphyry Mo mineralization.

Keywords: partition coefficient; porphyry molybdenum deposit; hydrothermal fluid; felsic melt;

*Corresponding author. E-mail: shanglinbo@vip.gyig.ac.cn

1. Introduction

Porphyry molybdenum deposits, the world's most important source of Mo, are commonly genetically related to high-K calc-alkaline granites generated by extensive fractional crystallization (Sinclair, 2007; Pettke et al., 2010; Sillitoe, 2010; Audétat and Li, 2017; Chen et al., 2017 and references therein). The efficient extraction of Mo from high-K calc-alkaline melt during the exsolution of magmatic fluids is an important step in Mo enrichment (Sinclair, 2007; Pettke et al., 2010; Sillitoe, 2010; Tattitch and Blundy, 2017). The partition coefficient of Mo between aqueous fluid and melt is a key parameter for quantitively understanding Mo enrichment in the process of hydrothermal fluid extraction from fractionated granitic melts. The coefficient is defined as $D_{Mo} = C_{Mo}^{fluid}/C_{Mo}^{melt}$, where C_{Mo}^{fluid} and C_{Mo}^{melt} are the concentrations of Mo in the aqueous fluid and melt, respectively.

Previous studies on the partition behaviors of Mo in natural and experimental samples have found that D_{Mo} varies from 0.06 to 135, with most values being less than 10 (Tingle and Fenn, 1984; Candela and Holland, 1984; Keppler and Wyllie, 1991; Chevychelov and Chevychelova, 1997; Webster, 1997; Bai and van Groos, 1999; Kravchuk, Malinin, 2000; Lerchbaumer and Audétat, 2013; Zajacz et al., 2008; Tattitch and Blundy, 2017). Generally, HCl, NaCl, and KCl in aqueous fluids can increase D_{Mo} (Keppler and Wyllie, 1991; Webster, 1997; Bai and van Groos, 1999; Schaefer et al., 1999; Tattitch and Blundy, 2017). In particular, in high-salinity brine ($NaCl_{eq}$ = 62 wt.%), D_{Mo} can reach up to 130 (Tattitch and Blundy, 2017). In contrast, HF in aqueous fluids has no discernible effect on D_{Mo} (Candela and Holland, 1984; Keppler and Wyllie, 1991).

Most of the melt used in previous experiments were peraluminous, and only a few experimental studies investigated the effect of the melt composition on the partition coefficient (Chevychelov and Chevychelova, 1997; Kracchuk et al., 2000). For example, with the melt composition changing from granodioritic to leucogranitic

(A/NK ratio from 1.53 to 1.32， where A/NK= (Al_2O_3)/ (Na_2O + K_2O) in mole), D_{Mo} values increases from 0.2 to 0.7 at 1 kbar and from 1.4 to 2.2 at 5 kbar, respectively (Chevychelov and Chevychelova 1997). There is no noticeable correlation between D_{Mo} and Al_2O_3 content of melts (Kracchuk et al., 2000).

To better understand the relationship between high-K calc-alkaline granites and Mo mineralization, we carried out equilibrium experiments on high silica melts with varying A/NK ratio and aqueous fluids with H_2O ± NaCl ± CO_2. The experimental results show that D_{Mo} increases with increasing alkalis and decreases with increasing A/NK in the melt. This study also demonstrates that coexisting fluid in highly evolved felsic magma has high potential for extracting Mo.

2. Method

2.1. Starting materials

The compositions of starting materials are given in Table 1. Felsic glasses were synthesized from dehydrated TEOS and high-purity Na_2CO_3, $KHCO_3$, and Al_2O_3. These samples were ground in an agate mortar to attain a grain size of <200 μm, and then mechanically mixed with about 600 ppm Mo in the form of high-purity MoO_3. Then, the powders (<2 grams) were placed into Pt crucibles and heated to 1350 °C at a rate of 150 °C/h. After annealing the powders at this temperature for 8 h, the Pt crucibles were quenched in cold water. The contained quenched glasses were ground several times in an agate mortar as starting materials.

Three different series of experiment with various fluid compositions were conducted in this study (Table 1): (1) the carbon dioxide series (X_{CO_2}= 0.096, 17.5 wt.% NaCl), (2) the water series (pure water with ~1000 ppm each of Rb, Cs, and B), and (3) the contrast series (11.73 wt.% NaCl and 8.34 wt.% KCl). Oxalate ($H_2C_2O_4$) was used to generate CO_2 (X_{CO_2}= 0.096) in the carbon dioxide series experiments and different content of water and solid NaCl were added to control the mole fractionation of CO_2.

Aqueous solutions containing various amounts of NaCl, KCl, RbCl, CsCl, and H_3BO_3 were prepared from analytical-grade chemicals and deionized water. The water series experiments were conducted in pure water containing 1000 ppm each of Cs, Rb, and B.

2.2. Experimental procedures

The capsule design is illustrated in Fig. 1. Approximately 200 mg of synthetized glasses and 200 mg of aqueous solutions as described above were loaded into gold capsules of 4.8 mm inner diameter (I.D.), 5.0 mm outer diameter (O.D.), and 25 mm length. The capsules were sealed with argon arc welding and placed in a drying oven (110 °C) for 24 h to check for potential leaks. Subsequently, the capsules were loaded into rapidly quenched cold-seal pressure vessels made of Ni-base alloy. All experiments were conducted at 850, 900 °C and 100 MPa, with water as pressure medium. Temperatures were measured with a K-type thermocouple in a hole at the end of the vessels. Pressures were measured with a Bourdon-type gauge with an uncertainty of 5 MPa. Oxygen fugacity was controlled by the material of the autoclave and was approximately the value of the nickel–nickel oxide (NNO) buffer (Chou, 1987). Based on previous experiments (e.g., Candela and Holland, 1984; Keppler and Wyllie, 1991; Webster, 1997; Tattitch and Blundy, 2017), a duration of 10 days was selected to guarantee experimental equilibrium. After these experimental durations, the vessels were rotated 90° to force the capsules to drop to the cold-water zone, and therefore allow the samples to reach room temperature within a few seconds. Capsules were then removed from the vessels, cleaned with dilute hydrochloric acid and deionized water, and then dried and weighed to determine whether the capsules had remained sealed during the experiments. Capsules with a mass change of less than 0.005 g were used for the subsequent analyses.

In the carbon dioxide series experiments, the quenched fluid and glass phases were separated following the procedure given by Wang et al. (2016). The pierced capsules were opened with surgical scissors, and then the opened capsules and quenched glasses

were eluted in 50 ml centrifuge tubes with 10% HNO_3 for 12 h. Molybdenum that was precipitated on the surfaces of Au capsules and quenched glasses was leached three times, and all of the leaching solutions were collected for ICP–MS analysis. The quenched glasses were ground to 200 mesh in an agate mortar for ICP–MS analysis, and the analyzed data of quenched glasses were defined as "bulk glass data".

For the water series and contrast series experiments, the quenched samples were treated using different procedures compared with the carbon dioxide series experiment. After quenching, dilute HCl solution was used to clean the surfaces of the gold capsules. The capsules were placed into liquid nitrogen for a few seconds to freeze the liquid inside and then cut using surgical scissors. The broken capsule was put into a Teflon beaker with 10 ml deionized water, and then annealed on an electric hot-plate at 80 ℃ for 8 h. This process was repeated three times, and all solutions were collected into a tube for analysis, similar to the procedure given by Guo et al. (2020). LA–ICP–MS was used to analyze the quenched glasses, which are free of fluid bubbles (Fig. 1). This strategy avoided the effect of such bubbles on the concentration of Mo in the glass phase, and the analyzed data were defined as "pure glass data". In addition, some of the quenched glasses (~20 mg) were also ground and analyzed using ICP-MS in the contrast series experiments. We compared values of D_{Mo} obtained from bulk glass data and pure glass data, which was used to evaluate the effect of bubbles containing in quenched glass on the concentration of Mo estimated using the different analytical methods.

2.3. Analysis of experimental products

Major elements of synthetic glasses were analyzed using LA–ICP–MS at the State Key Laboratory of Ore Deposit Geochemistry, Institute of Geochemistry Chinese Academy of Sciences, Guiyang, China. The Mo concentrations of quenched glasses (the carbon dioxide series and the contrast series) and leaching solutions were analyzed by a Finnigan MAT ELEMENT ICP–MS instrument using the procedures described by

Qi et al. (2000) at the State Key Laboratory of Ore Deposit Geochemistry. A working curve using standard solutions of different concentrations was utilized to calculate absolute concentrations of Mo in quenched glasses and leaching solutions. Rhodium was used as an internal standard to monitor signal drift during counting.

For the water series and contrast series experiments, the quenched glasses without fluid inclusions were analyzed by LA–ICP–MS. Laser sampling was performed using a GeoLas Pro 193 nm ArF excimer laser. An Agilent 7900 ICP–MS instrument was used to acquire ion-signal intensities. Helium was used as the carrier gas, which was mixed with Argon via a T-connector before entering the ICP–MS instrument. Each analysis incorporated a background acquisition of approximately 30 s (gas blank) followed by 50 s of data acquisition from the sample. Element concentrations were calibrated against multiple reference materials (NIST 610, BCR-2G, BIR-1G, and BHVO-2G) without applying internal standardization (Liu et al., 2008). Off-line selection and integration of background and analyte signals, as well as time-drift correction and quantitative calibration, were performed using ICPMSDataCal (Liu et al., 2008).

3. Results

All of the data of the carbon dioxide series, pure water series, and contrast series experiments are reported in Table 2. The ratio A/NK was used to quantify the composition of felsic melts. The results of this study show that D_{Mo} in all cases decreases with increasing A/NK and D_{Mo} is generally higher in the carbon dioxide series than that in the pure water series (Fig. 2a and b).

In the carbon dioxide series, D_{Mo} decreases from 4.13 to 0.56 as the molar ratio of A/NK increases from 0.75 to 1.36 under conditions of the starting solution containing X_{CO_2}= 0.096 and 17.5 wt.% NaCl (Fig. 2a). A typical double-eyelid structure of fluid inclusions containing CO_2 appears in the quenched melt of the carbon dioxide series

(Fig. 1). We also analyzed fluid inclusions of the sample using Raman spectroscopy, which showed the presence of CO_2 (Fig. 1).

For the water series, all values of D_{Mo} are below 1.0 (Table 2), and D_{Mo} decreases from 0.54 to 0.15 as A/NK increases from 0.72 to 1.23 (Fig. 2b). Compared with D_{Mo} of the carbon dioxide series, D_{Mo} in the water series at the same A/NK is smaller, which suggests that the salinity of the carbon dioxide series enhances the extraction of Mo from the melt phase into fluids.

Quenched glasses of the water series and contrast series experiments were randomly analyzed by LA–ICP–MS. As revealed in the data listed in Table 3, the relative standard deviation (RSD) of major element contents was very small (typically <0.5%), and the RSD of the concentration of Mo was slightly higher, but with the maximum being <20% and most analyses being <10%. These results suggest that all the elements in quenched glasses are homogeneous in content and also confirm that experimental equilibrium attained in 10 days.

For the contrast series, the partition coefficients that were calculated on the basis of the concentration of Mo in the bulk glasses and pure glasses data coincide (Table 2), which demonstrates that in our experiments, there was a negligible effect of trapped bubbles on the concentration of Mo in silicate glasses, and therefore the Mo concentration data from quenched glass obtained from ICP-MS can be used to represent the concentration of Mo in melts.

The sources of experimental error involve two main aspects. First, it may be hard to remove all precipitated Mo from the surface of Au capsules and quenched glasses. However, the experiments conducted by Borchert et al. (2010a, 2010b) showed a good correlation in element concentration between leaching solutions and in situ determined fluid. In this study, we used the same method to leach Mo from capsules in the water series experiments. Therefore, the precipitated Mo in quenched glasses and Au capsules

has little effect on the concentration of Mo in the fluid. Second, when melt cools through the glass transition temperature, some fluid will be trapped as glass-hosted fluid inclusions (Romano et al., 1994, Simon et al., 2007). In the present study, we found from the double-polished wafer that only 1 vol.% fluid phase was trapped in quenched glass (Fig. 1). The contrast series experiments were conducted to estimate the experimental error from the trapped fluid on the Mo concentration of quenched glasses. LA-ICP-MS was used to analyze the quenched glasses without bubbles, and ICP-MS was used to analyze the ground quenched glasses containing fluid bubbles. The results show that values of D_{Mo} calculated using the two different methods (pure glasses or bulk glasses) coincide on the whole, and the deviation is in the range of the experiment error. (Table 2).

4. Discussion

4.1. Comparison with previous results

As mentioned above, values of D_{Mo} in natural and experimental samples encompass a wide range from 0.06 to 135 (Fig. 3a), but are mostly <10. In situ composition analyses of fluid and melt inclusions in quartz from intrusions of porphyry Mo deposits have shown that D_{Mo} values of natural samples were in all cases larger than 1, varying from 1 to 24, with the melt compositions being metaluminous and slightly peralkaline (A/CNK [A/CNK=Al_2O_3/ (CaO + Na_2O + K_2O) in mole] ranging from 0.9 to 1.1) (Audétat et al., 2008; Zajacz et al., 2008; Audétat, 2010; Lerchbaumer and Audétat; 2013). The relationship of D_{Mo} versus A/CNK from natural samples shows that D_{Mo} is high for melts with low A/CNK relatively.

Some previous experiments confirmed the influence of melt composition on D_{Mo}. Chevychelov and Chevychelova (1997) reported values of D_{Mo} for aqueous fluids (H_2O–NaCl–HCl) and various synthetic gels. All of the gels were peraluminous and contained 5.2 wt.% CaO in granodioritic gel and 2.0 wt.% CaO in leucogranitic gel. D_{Mo} decreased with increasing A/NK at around 900 °C. Specifically, D_{Mo} ranged from

0.65 to 0.25 at 100 MPa and from 2.1 to 1.45 at 500 MPa. Kravchuk et al. (2000) conducted experiments to study D_{Mo} between fluid with 1m NaCl and various synthetic melts under conditions of 800 °C and 1.0–2.0 kbar. The melts were prepared using albite and other peraluminous glasses. We reprocessed their experimental data and found that D_{Mo} decreased from 7.33 at A/NK = 0.98 to 0.22 at A/NK = 1.52 (Fig. 3b). Our experimental results clearly show the same trend of D_{Mo} increasing with decreasing A/NK, and values of D_{Mo} are in the established range for natural samples (Fig. 3b).

The main differences between our experiments and those of Chevychelov and Chevychelova (1997) and Kravchuk et al. (2000) were that our starting melt did not contain CaO and some of comparison experiments were conducted at higher pressure (e.g., 500 MPa). In addition, the melt composition of Chevychelov and Chevychelova (1997) and Kravchuk et al. (2000) were peraluminous, and only the highest value of D_{Mo} of 7.33 was obtained using albite as the starting melt, which may be caused by the degree of polymerization of albite. This is because albite is fully polymerized, the solubility of molybdenite in highly polymerized melts is very low (Isuk, 1983), which will allow more Mo to dissolve into the coexisting solution, in turn leading to a high D_{Mo}. In some of our experiments, D_{Mo} is very small (e.g., 0.25) and may be explained by the existence of CaO in the melt and the starting solution didn't contain salinity. CaO is known to prevent Mo from being distributed into magmatic fluids (Kravchuk et al., 2000), although Chevychelov and Chevychelova (1997) considered that Ca enhances the concentration of Mo in fluids and is precipitated as a crystalline phase. In contrast, magma forming porphyry Mo is in all cases highly evolved, and the melt composition is high-K calc-alkaline. The data of Chevychelov and Chevychelova (1997) and Kravchuk et al. (2000) obtained from peraluminous melt cannot explain the relationship between the causative magma and high-K calc-alkaline granite.

We also note that fluid salinity affects D_{Mo} in both natural and experimental samples. The highest reported value of D_{Mo} can reach 135 in hypersaline fluids (Tattitch and Blundy, 2017), which is in good agreement with results from an earlier experiment

(Webster, 1997). In a system involving low to medium salinity fluids, values of D_{Mo} are in all cases less than 10. In our study, carbon dioxide series experiments using fluids with 17.5 wt.% NaCl resulted in higher D_{Mo} values than those of the pure water series.

4.2. Effect of melt composition on D_{Mo}

Our results reveal that D_{Mo} decreases with increasing A/NK and that D_{Mo} is higher in peralkaline melts than that in peraluminous melts, which can be attributed to the change of the structure of melt and the Mo species in melt.

The basic units of felsic melts are a silicon–oxygen tetrahedron and an aluminum–oxygen tetrahedron. The oxygen linking the Si^{4+} "network-forming" cations is denoted as "bridging O" (BO), and the oxygen linking Si^{4+} and other cations (network-modifying) is denoted as "non-bridging oxygen" (NBO). The ratio NBO/T is defined by Equation (1), in which all elements are represented as molar concentrations in silicate melt (Mysen, 1988):

$$NBO/T = (2 \times A - 4 \times T)/T \quad (1)$$

where T represents the total number of tetrahedral central cations, and A represents the total number of anions. Mo is present primarily as molybdate moieties ($Mo(VI)O_4^{2-}$) in most silicate melt (Farges et al., 2006), which suggests that chemically active oxygen, also referred to as NBO, would be required to form the molybdate moieties in melt.

In peraluminous melt, there are two types of aluminum: one type that forms Al–O–Al tetrahedra with charge-balancing cations; and another type that modifies the silicate network, acting as network-modifying cations and decreasing the degree of polymerization and increasing the number of NBOs of silicate melt (Stebbins, 2016). The increasing number of NBOs in melt favors the formation of molybdate moieties and leads to a decrease in D_{Mo}.

In our experiments, D_{Mo} is higher in all cases for the peralkaline melts than for the peraluminous melts, even for the same NBO/T (Fig. 2c and d). In addition, D_{Mo} increases with an increasing alkali content of melt (Fig. 2e and f). In the peralkaline melt, the excess alkali and alkaline earth metal ions may form complexes with the molybdate moieties to form Na_2MoO_4, K_2MoO_4, or $CaMoO_4$ (Farges, 2006; O'Neill and Eggins, 2002). D_{Mo} is controlled predominantly by the nucleation of molybdate rather than the NBO/T ratio of the melt (Fig. 2c and d). Molybdate is the main species of Mo in saline fluids (Cao, 1989; Kudrin, 1989; Bali et al., 2012; Zhang et al., 2012; Tattitch and Blundy, 2017; Shang et al., 2020). The higher salinity in our carbon dioxide series relative to the other experiments enhances the solubility of molybdate moieties such as Na_2MoO_4 and K_2MoO_4 in fluids and increased D_{Mo}. $NaMoO_3Cl$ is favored as the main species in hypersaline fluids (Tattitch and Blundy, 2017).

A trend similar to that observed for the carbon dioxide series was investigated in the water series experiments (Fig. 2b and d), whereby in peraluminous melt, D_{Mo} decreases with increasing NBO/T. In contrast, in peralkaline melt, D_{Mo} increases with increasing NBO/T, where the nucleation of Na_2MoO_4 and K_2MoO_4 is a critical factor, as the solubility of molybdate controls the partition of Mo between melt and coexisting fluids. In other words, peralkaline residual magma can promote the partitioning of Mo into hydrothermal fluids.

4.3. Implications for porphyry deposits

During the evolution of a porphyry system, exsolved fluid will extract metallogenic metals from magma and transport them to the shallow crust, where they are precipitated to form a porphyry deposit (Sinclair, 2007). In the early stage of the formation of Mo deposits, the degree of evolution of felsic magma is low and the magma contains large amounts of volatiles and NBOs, resulting in a relatively small D_{Mo} between fluid and melt. At the same stage, the viscosity of magma is very low, and large volumes of magma are easy to form (Zhang and Audétat, 2017). Subsequently, the residual melt

will undergo Mo enrichment as the magma ascends to the shallow crust and crystallization differentiation occurs (Wang et al., 2014; Zhang and Audétat, 2017). If the magma undergoes sufficient crystal–melt segregation, such as the crystallization of amphibole (Du and Audétat, 2020), the residual melt will be depleted in aluminum and enriched in alkalis. Similar magma compositional variations may be induced by assimilating alkali-rich strata or by mixing with an alkali-rich magma injected into the magma chamber. With decreasing A/NK of the residual melt, D_{Mo} will increase markedly, and more Mo will be distributed into coexisting fluids.

To evaluate the effect of melt composition on the formation of porphyry Mo deposits, we modeled fluid exsolution processes in the magma chamber. In a hypocritical felsic chamber, we assumed that the magma volume is about 100 km^3, the concentration of Mo is 15 ppm (Audétat and Li, 2017, and references therein), the water content of the magma is about 5 wt.%, and the magma density is 2.5 g/cm^3. Molybdenum may be hypothetically deposited in a hydrothermal environment with 100% precipitation efficiency (Pokrovski et al., 2013). The amount of Mo in the magmatic fluid is thus essential for the grade and scale of porphyry Mo deposits. Using the partition coefficients established in the present study, simple mass balance calculations show that carbon dioxide saline solution (850 °C, 100 MPa, X_{CO_2}= 0.096, and 17.5 wt.% NaCl) extracts about 6.3 times more Mo from peralkaline magma (for A/NK = 0.75 and 51.35 ppm Mo in the fluid phase, 6.4×10^5 ton of Mo will be deposited in the porphyry metallogenic stage) than from peraluminous magma (for A/NK = 1.2 and 8.17 ppm Mo in the fluid phase, 1.1×10^5 ton of Mo will be deposited in the porphyry metallogenic stage). For fluid composed of pure water (900 °C and 100 MPa), the fluid can extract about 3.5 times more Mo from peralkaline magma (A/NK = 0.72, 7.88 ppm Mo in the fluid phase, 9.8×10^4 ton Mo) than from peraluminous magma (A/NK = 1.23, 2.23 ppm Mo in the fluid phase, 2.8×10^4 ton Mo) in a closed system. Therefore, a porphyry magma containing excess alkali is a key factor for Mo enrichment and for forming a granite-related Mo ore deposit. Furthermore, we also used the Rayleigh fractionation

model to calculate the efficiency of Mo extracted from magma by fluids (Fig. 4). According to our calculations, in the case where 10% of the fluid is extracted from felsic magma, the concentration of Mo in coexisting fluid is 1058 ppm (D_{Mo}= 4.13, A/NK = 0.75). In the case where D_{Mo} changes to 0.56 (A/NK = 1.2), as obtained for peraluminous melt, the concentration of Mo in coexisting fluid is 171 ppm. The Rayleigh fractionation calculation is consistent with our mass balance calculation results, supporting our interpretation that a peralkaline melt composition favors the formation of porphyry Mo deposits.

A highly evolved magma that is enriched in alkali favors more Mo being distributed into coexisting magmatic fluids, which can explain why magma forming porphyry Mo deposits is typically highly evolved.

5. Conclusion

Our experimental results show that the partition coefficient of Mo between fluid and felsic melt (D_{Mo}) decreases with increasing A/NK in melt. D_{Mo} is higher in peralkaline melt than in peraluminous melt, and peralkaline melt is therefore more favorable for the enrichment of Mo during magmatic–hydrothermal processes. This finding improves our understanding of the transport of Mo in magmatic–hydrothermal systems. Any geological processes that act to increase the alkali concentration of melts, such as crystal–melt segregation (e.g., amphibole), assimilation of alkali-rich strata into the magma, and mixing with alkali-rich magma in the magma chamber, favor the formation of porphyry Mo deposits.

Acknowledgments

Financial support for the study was provided by the National Key Research and Development Program of China (2016YFC0600204), the National Natural Science Foundation of China (U1812402, 41673067, and 91955209), and the Open Research Fund of the State Key Laboratory of Ore Deposit Geochemistry to Haihao Guo. We gratefully acknowledge the help of Yanwen Tang and Yinghua Chen during LA–ICP–MS analyses, and Jin Hu and Yan Huang in conducting ICP–MS analyses.

Reference

Audétat, A., 2010. Source and Evolution of Molybdenum in the Porphyry Mo(-Nb) Deposit at Cave Peak, Texas. J Petrol. 51:1739-1760.

Audétat, A., Li, W., 2017. The genesis of Climax-type porphyry Mo deposits: Insights from fluid inclusions and melt inclusions. Ore Geol. Rev. 88:436-460.

Audétat, A., Pettke, T., Heinrich, CA., Bodnar, RJ., 2008. The Composition of Magmatic-Hydrothermal Fluids in Barren and Mineralized Intrusions. Econ. Geol. 103:877-908.

Bai, TB., van Groos, AFK., 1999. The distribution of Na, K, Rb, Sr, Al, Ge, Cu, W, Mo, La, and Ce between granitic melts and coexisting aqueous fluids. Geochim. Cosmochim. Acta 63:1117-1131.

Bali, E., Keppler, H., Aud Audétat tat, A., 2012. The mobility of W and Mo in subduction zone fluids and the Mo–W–Th–U systematics of island arc magmas. Earth Planet Sc Lett. 351–352:195-207.

Borchert, M., Wilke, M., Schmidt, C., Cauzid, J., Tucoulou, R., 2010a. Partitioning of Ba, La, Yb and Y between haplogranitic melts and aqueous solutions: An experimental study. Chem. Geol. 276:225-240.

Borchert, M., Wilke, M., Schmidt, C., Rickers, K., 2010b. Rb and Sr partitioning between haplogranitic melts and aqueous solutions. Geochim. Cosmochim. Acta. 74:1057-1076.

Candela, PA., Holland, HD., 1984. The partitioning of copper and molybdenum between silicate melts and aqueous fluids. Geochim. Cosmochim. Acta. 48:373-380.

Cao, X., 1989. Solubility of molybdenite and the transport of molybdenum in hydrothermal solutions.

Chen, Y-J., Wang, P., Li, N., Yang, Y-F., Pirajno, F., 2017. The collision-type porphyry Mo deposits in Dabie Shan, China. Ore Geol. Rev. 81:405-430.

Chevychelov, V., Chcvychelova, TK., 1997. Partitioning of Pb, Zn, W, Mo, CI, and major elements between aqueous fluid and melt in the systems granodiorite (granite, leucogranite)-H_2O-NaCl-HCl. Neues Jahrbuch für Mineralogie-Abhandlungen. 172:101-115.

Chou, I-M., 1987. Oxygen buffer and hydrogen sensor techniques at elevated pressures and temperatures. Hydrothermal experimental techniques. 61-99.

Du J, Audétat A. 2020. Early sulfide saturation is not detrimental to porphyry Cu-Au formation. Geology. 48, 519-524

Farges, F., Siewert, R., Brown, GE., Guesdon, A., Morin, G., 2006. Structural environments around molybdenum in silicate glasses and melts. I. Influence of composition and oxygen fugacity on the local structure of molybdenum. Can. Mineral. 44:731-753.

Guo, H., Xia, Y., Bai, R., Zhang, X., Huang, F., 2020. Experiments on Cu-isotope fractionation between chlorine-bearing fluid and silicate magma: implications for fluid exsolution and porphyry Cu deposits. Natl. Sci. Rev. 0:1-12.

Isuk, EE., 1983. Behavior of molybdenum in alkali silicate melts: Effects of excess SiO_2 and CO_2. Lithos. 16:17-22.

Keppler, H., Wyllie, PJ., 1991. Partitioning of Cu, Sn, Mo, W, U, and Th between melt and aqueous fluid in the systems haplogranite-H_2O−HCl and haplogranite-H_2O−HF. Contrib. Mineral. Petrol. 109:139-150.

Khitarov, NI., Malinin, SD., Lebedev, EB., Shibaeva, NP., 1982. Partition of Zn, Cu, Pb and Mo between the fluid phase and silicate melt of granitic composition under high-temperature and pressure. Geokhimiya. 8:1094-1107.

Kravchuk, I., Malinin, S., Senin, V., Dernov-Pegarev, V., 2000. Molybdenum partition between melts of natural and synthetic aluminosilicates and aqueous-salt fluids. Geochem. Int. 38:130-137.

Kudrin, A., 1989. Behavior of Mo in aqueous NaCl and KCl solutions at 300–450 °C. Geochem. Int. 26:87-99.

Lerchbaumer, L., Aud Audétat, A., 2013. The Metal Content of Silicate Melts and Aqueous Fluids in Subeconomically Mo Mineralized Granites: Implications for Porphyry Mo Genesis. Econ. Geol. 108:987-1013.

Li, N., Ulrich, T., Chen, Y-J., Thomsen, TB., Pease, V., Pirajno, F., 2012. Fluid evolution of the Yuchiling porphyry Mo deposit, East Qinling, China. Ore Geol. Rev. 48:442-459.

Liu, Y., Hu, Z., Gao, S., Gunther, D., Xu, J., Gao, C, et al., 2008. In situ analysis of major and trace elements of anhydrous minerals by LA-ICP-MS without applying an internal standard. Chem. Geol. 257:34-43.

Mysen, BO. 1988. Structure and properties of silicate melts.

O'Neill, HSC., Eggins, SM., 2002. The effect of melt composition on trace element partitioning: an experimental investigation of the activity coefficients of FeO, NiO, CoO, MoO_2 and MoO_3 in silicate melts. Chem. Geol. 186:151-181.

Pettke, T., Oberli, F., Heinrich, CA., 2010. The magma and metal source of giant porphyry-type ore deposits, based on lead isotope microanalysis of individual fluid inclusions. Earth Planet Sc Lett. 296:267-277.

Pokrovski, GS., Borisova, AY., Bychkov, AY. 2013. Speciation and Transport of Metals and Metalloids in Geological Vapors. Rev Mineral Geochem. 76:165-218.

Qi, L., Hu, J., Gregoire, DCJT., 2000. Determination of trace elements in granites by inductively coupled plasma mass spectrometry. Talanta. 51:507-513.

Romano, C., Dingwell, DB., Sterner, SMJAM., 1994. Kinetics of quenching of hydrous feldspathic melts: quantification using synthetic fluid inclusions. Am. Mineral. 79:1125-1134.

Schaefer, B., Frischknecht, R., Guenther, D., Dingwell, DB., 1999. Determination of trace-element partitioning between fluid and melt using LA-ICP-MS analysis of synthetic fluid inclusions in glass. Eur. J Mineral. 11:415-426.

Shang, L., Williams-Jones, AE., Wang, X., Timofeev, A., Hu, R., Bi, X., 2020. An Experimental Study of the Solubility and Speciation of MoO_3(s) in Hydrothermal Fluids at Temperatures up to 350 °C. Econ. Geol. 115:661-669.

Sillitoe, RH., 2010. Porphyry Copper Systems. Econ. Geol. 105:3-41.

Simon, AC., Frank, MR., Pettke, T., Candela, PA., Piccoli, PM., Heinrich, CA, et al., 2007. An evaluation of synthetic fluid inclusions for the purpose of trapping equilibrated, coexisting, immiscible fluid phases at magmatic conditions. Am. Mineral. 92:124-138.

Sinclair, WD., 2007. Porphyry deposits:Mineral deposits of Canada: A synthesis of major deposit-types, district metallogeny, the evolution of geological provinces, exploration methods: Geological Association of Canada. Mineral Deposits Division, Special Publication. 5:223-243.

Stebbins, JF., 2016. Glass structure, melt structure, and dynamics: Some concepts for petrology. Am. Mineral. 101:753-768.

Tattitch, BC., Blundy, JD., 2017. Cu-Mo partitioning between felsic melts and saline-aqueous fluids as a function of X_{NaCleq}, f_{O2}, and f_{S2}. Am. Mineral. 102:1987-2006.

Tingle, TN., Fenn, PM., 1984. Transport and concentration of molybdenum in granite molybdenite systems: Effects of fluorine and sulfur. Geology. 12:156-158.

Ulrich, T., Mavrogenes, J., 2008. An experimental study of the solubility of molybdenum in H_2O and KCl–H_2O solutions from 500 °C to 800 °C, and 150 to 300 MPa. Geochim. Cosmochim. Acta 72:2316-2330.

Wang, G-G., Ni, P., Yu, W., Chen, H., Jiang, L-L., Wang, B-H, et al., 2014. Petrogenesis of Early Cretaceous post-collisional granitoids at Shapinggou, Dabie Orogen: Implications for crustal architecture and porphyry Mo mineralization. Lithos. 184:393-415.

Wang, S., Li, H., Shang, L., Bi, X., Wang, X., Fan, W., 2016. Copper partitioning between granitic silicate melt and coexisting aqueous fluid at 850 ℃ and 100 MPa. Acta Geochimica. 35:381-390.

Webster, JD., 1997. Exsolution of magmatic volatile phases from Cl-enriched mineralizing granitic magmas and implications for ore metal transport. Geochim. Cosmochim. Acta. 61:1017-1029.

Zajacz, Z., Halter, WE., Pettke, T., Guillong, M., 2008. Determination of fluid/melt partition coefficients by LA-ICPMS analysis of co-existing fluid and silicate melt inclusions: Controls on element partitioning. Geochim. Cosmochim. Acta. 72:2169-2197.

Zhang, D., Audétat, A., 2017. Chemistry, Mineralogy and Crystallization Conditions of Porphyry Mo-forming Magmas at Urad–Henderson and Silver Creek, Colorado, USA. J Petrol. 58:277-296.

Zhang, L., Audétat, A., Dolejš, D., 2012. Solubility of molybdenite (MoS_2) in aqueous fluids at 600–800 °C, 200 MPa: A synthetic fluid inclusion study. Geochim. Cosmochim. Acta. 77:175-185.

Captions for Figures and Tables

Fig. 1 The experimental process and sample assembly used for this study. Pure gold was used for the capsule for the experiments. The capsule was filled with synthetic glass and aqueous solution. The photomicrograph shows double-polished quenched glass. Raman spectroscopy verified the existence of CO_2.

Fig. 2 The relationship between D_{Mo} and A/NK, NBO/T, and $Na_2O + K_2O$, where A/NK is calculated as $Al_2O_3/(Na_2O + K_2O)$ (in mole of the starting materials), and $Na_2O + K_2O$ is in wt.%. (a) shows the variation in D_{Mo} for the carbon dioxide series experiments. The concentration of Mo in quenched glasses was analyzed by dissolving the glass in HNO_3 and HF and then using ICP–MS for analysis. Error bars are smaller than the scale of the icons. (b) shows the variation in D_{Mo} for the water series experiments. The concentration of Mo in quenched glasses was analyzed using LA–ICP–MS. The dotted red frame represents D_{Mo} in peralkaline melt (d), and the dotted blue frame represents D_{Mo} in peraluminous melt (c and d). (e) and (f) show variation in D_{Mo} with respect to the alkali concentration of melt in carbon dioxide series and water series.

Fig. 3 (a) Experimental partition coefficients collected from Khitarov et al. (1982), Candela and Holland (1984), Tingle and Fenn (1984), Keppler and Wyllie (1991), Chevychelov and Chevychelova (1997), Webster (1997), Bai and van Groos (1999), Schaefer et al. (1999), Kravchuk and Malinin (2000), Tattitch and Blundy (2017), and this study. Melt and fluid compositions differ among studies. Values of the partition coefficient for natural samples were collected from Zajacz et al. (2008), Audétat et al. (2008), Audétat (2010), and Lerchbaumer and Audétat (2013). (b) A comparison of experimental data between the present study and Chevychelov and Chevychelova (1997) and Kravchuk et al. (2000). A/NK is the molar ratio of Al_2O_3 / $(Na_2O + K_2O)$ in the starting materials. Solid blue circles and squares represent the carbon dioxide series (fluid composition of H_2O-NaCl-CO_2) and water series (pure water containing 1000 ppm each of Rb, Cs, and B) experiments, respectively. Unfilled blue diamonds

represent experimental data from Kravchuk et al. (2000). Unfilled red hexagons represent experimental data from Chevychelov and Chevychelova (1997) at 1 kbar, and hexagons with a cross represent their experiments conducted at 5 kbar.

Fig. 4 A schematic illustrating the exsolution of fluid from magma (left), and the concentration of Mo in coexisting fluid calculated using Rayleigh fractionation with different partition coefficients (right). For the right-hand diagram, the x-axis represents the degree of extraction of fluid from melt, and the y-axis represents the concentration of Mo in coexisting fluids. In Rayleigh fractionation, "F" represents the extraction ratio of fluid, so (1 – F) was used to calculate the concentration of Mo in residual felsic magma.

Table 1 Starting materials of the three series of experiments.

Table 2 Element concentrations of quenched glasses and solutions, and the calculated distribution coefficient (D_{Mo}) between solutions and quenched glasses.

Table 3 The average composition and relative standard deviation (RSD) of quenched glasses of the contrast and water series glasses using data obtained at randomly selected points using LA–ICP–MS.

Figures

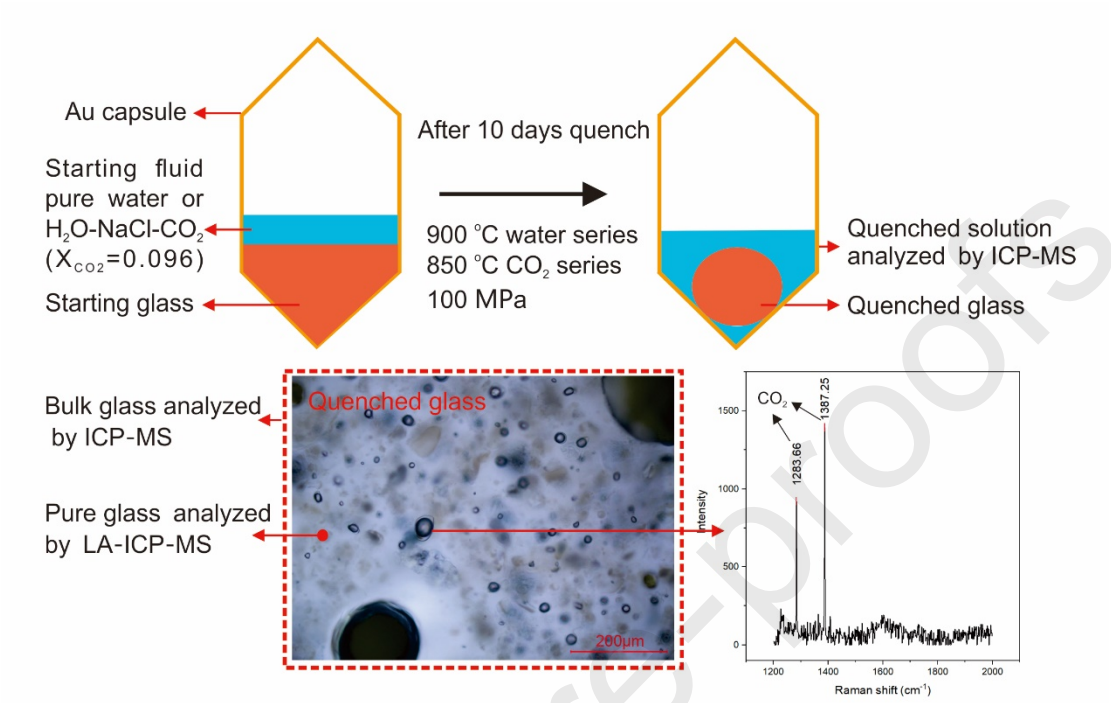

Fig. 1.

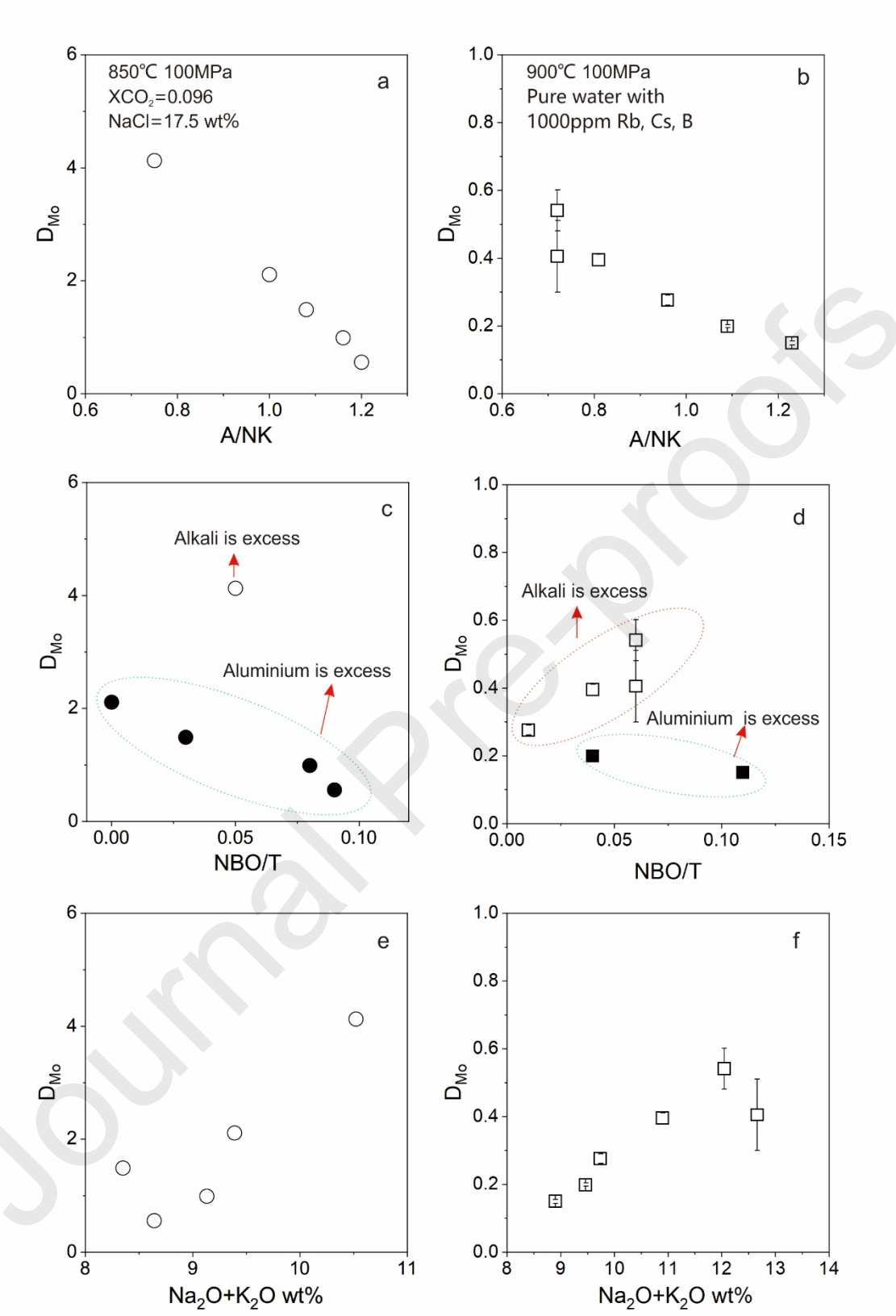
850℃ 100MPa
XCO2=0.096
NaCl=17.5 wt%
a
DMo
A/NK
900℃ 100MPa
Pure water with
1000ppm Rb, Cs, B
b
DMo
A/NK
c
Alkali is excess
Aluminium is excess
DMo
NBO/T
d
Alkali is excess
Aluminium is excess
DMo
NBO/T
e
DMo
Na2O+K2O wt%
f
DMo
Na2O+K2O wt%

Fig. 2.

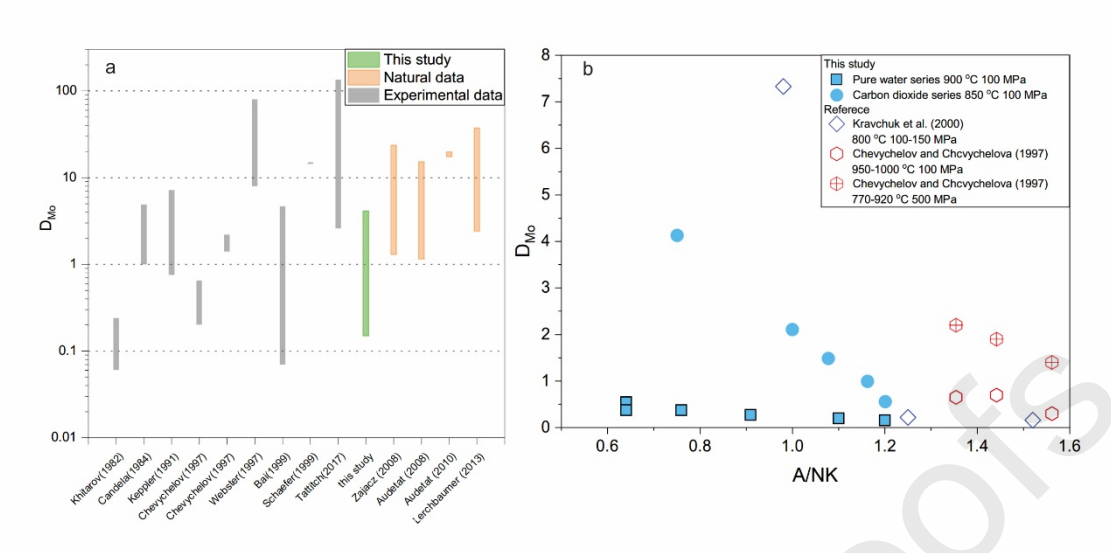

Fig. 3.

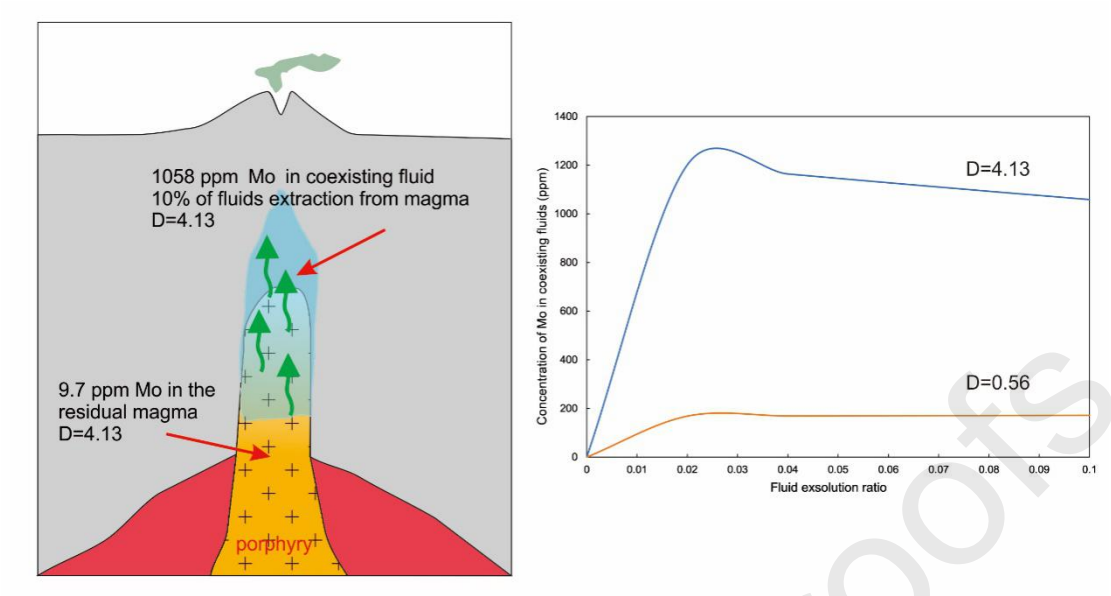

Fig. 4.

Table 1

Starting materials of the three experiments

Run	T °C	P MPa	Na_2O wt.%	Al_2O_3 wt.%	SiO_2 wt.%	K_2O wt.%	A/NK	NBO/T	Mo ppm
The carbon dioxide series (X_{CO_2}= 0.096, 17.5wt.% NaCl)									
M1-1	850	100	5.47	10.86	78.12	5.05	0.75	0.05	952
M1-2	850	100	4.47	12.46	78.20	3.88	1.08	0.03	805
M1-3	850	100	5.12	13.05	76.00	4.27	1.00	0.00	693
M1-4	850	100	4.70	14.42	75.88	3.94	1.20	0.09	717
M1-6	850	100	5.45	15.06	75.70	3.68	1.16	0.08	576
The water series (pure water with 1000ppm Rb, Cs, B)									
J-039	900	100	5.28	11.10	77.12	6.41	0.71	0.06	592
J-040	900	100	5.01	11.86	77.08	5.98	0.81	0.04	497
J-041	900	100	4.23	14.25	76.15	5.30	1.12	0.06	529
J-042	900	100	3.92	12.44	77.59	5.95	0.96	0.01	656
J-043	900	100	3.99	15.26	75.61	5.06	1.27	0.13	591
J-044	900	100	5.28	11.10	77.12	6.41	0.71	0.06	592
The contrast series (11.73 wt.% NaCl, 8.34 wt.% KCl)									
J-003	900	100	4.23	14.25	76.15	5.30	1.12	0.06	529
J-010	900	100	3.99	15.26	75.61	5.06	1.27	0.13	591
J-016	900	100	5.28	11.10	77.12	6.41	0.71	0.06	592

A/NK= $(Al_2O_3)/ (Na_2O + K_2O)$ in mole; $X_{CO_2}= CO_2/ (CO_2 + H_2O)$ in mole; NBO/T is the ratio of non-bridge oxygen to tetrahedron ions, as defined in the discussion section (4.2). The concentrations in parentheses are those of the starting solutions.

Table 2

Compositions of quenched glasses and leaching solution, and the calculated partition coefficient (D_{Mo}) between leaching solution and quenched glasses.

Run.	Na_2O wt.%	Al_2O_3 wt.%	SiO_2 wt.%	K_2O wt.%	A/NK	NBO/T	Mo ppm Quenched solution[a]	Mo ppm Bulk glasses[b]	Mo ppm Pure glasses[c]	σ	D_{Mo} Bulk	D_{Mo} Pure	D_{Mo} σ
The carbon dioxide series													
M1-1	n.a.	n.a.	n.a.	n.a.	0.75	0.05	861	208	n.a.		4.13	n.a.	
M1-2	n.a.	n.a.	n.a.	n.a.	1.08	0.03	539	363	n.a.		1.49	n.a.	
M1-3	n.a.	n.a.	n.a.	n.a.	1.00	0.00	367	174	n.a.		2.11	n.a.	
M1-4	n.a.	n.a.	n.a.	n.a.	1.20	0.09	240	428	n.a.		0.56	n.a.	
M1-6	n.a.	n.a.	n.a.	n.a.	1.16	0.08	353	356	n.a.		0.99	n.a.	
The water series													
J-039	5.40	11.52	75.56	6.65	0.72	0.06	174	n.a.	322	36.0	n.a.	0.54	0.06
J-040	4.78	11.74	76.61	6.12	0.81	0.04	124	n.a.	315	13.0	n.a.	0.39	0.02
J-041	4.11	13.67	76.09	5.36	1.09	0.04	96	n.a.	482	10.8	n.a.	0.20	0.00
J-042	3.76	12.19	77.22	5.98	0.96	0.01	139	n.a.	503	25.7	n.a.	0.28	0.01
J-043	3.89	14.61	75.67	5.01	1.23	0.11	78	n.a.	521	19.5	n.a.	0.15	0.01
J-044	5.63	12.14	74.21	7.03	0.72	0.06	136	n.a.	337	87.8	n.a.	0.40	0.11
The contrast series													
J-003	5.12	14.20	73.96	6.61	0.91	0.02	121	302	351	19.4	0.40	0.34	0.02
J-010	4.51	14.36	74.70	6.28	1.01	0.00	203	437	492	20.3	0.46	0.41	0.02

J-016	6.09	12.08	72.45	9.35	0.60	0.11	238	56	47	8.20	4.23	5.07	0.89

Notes: [a] The concentration of Mo in the fluid phase. All leaching solution was collected and then analyzed using ICP–MS.

[b] The concentration of Mo in quenched glass. The glass was dissolved by HNO_3 and HF and then analyzed using ICP–MS.

[c] The concentration of Mo in quenched glass. LA–ICP–MS was used to avoid analyzing the fluid phase that was trapped in quenched glasses.

σ represents the 1 sigma standard deviation of the measurements.

D_{Mo} bulk means that the partition coefficient was calculated using a/b.

D_{Mo} pure means the partition coefficient was calculated using a/c.

n.a. data were not analyzed.

Table 3

The average composition and the relative standard deviation (RSD) of the quenched glasses of the contrast and water series glasses at randomly different points using LA-ICP-MS.

		Na_2O			Al_2O_3			SiO_2			K_2O			Mo		
	N	wt.%	σ	RSD	wt.%	σ	RSD	wt.%	σ	RSD	wt.%	σ	RSD	ppm	σ	RSD
The water series																
J-039	3	5.40	0.06	1.05	11.52	0.11	0.97	75.56	0.23	0.30	6.65	0.03	0.51	322	36.0	9.93
J-040	7	4.78	0.02	0.50	11.74	0.02	0.20	76.61	0.07	0.10	6.12	0.05	0.80	315	13.0	7.29
J-041	5	4.11	0.10	2.31	13.67	0.29	2.10	76.09	0.45	0.59	5.36	0.07	1.35	482	10.8	2.25
J-042	5	3.76	0.06	1.68	12.19	0.18	1.45	77.22	0.28	0.36	5.98	0.10	1.70	503	25.7	5.10
J-043	5	3.89	0.03	0.84	14.61	0.14	0.99	75.67	0.16	0.21	5.01	0.06	1.11	521	19.5	3.74
J-044	4	5.63	0.08	1.35	12.14	0.82	6.79	74.21	0.99	1.33	7.03	0.19	2.72	337	87.8	3.20
The contrast series																
J-003	6	5.14	0.07	1.32	14.20	0.22	1.58	73.89	0.45	0.60	6.66	0.21	3.09	351	19.4	5.51
J-010	10	4.53	0.08	1.77	14.48	0.24	1.66	74.49	0.37	0.49	6.34	0.15	2.42	492	20.3	4.15
J-016	6	6.10	0.05	0.80	12.01	0.25	2.05	72.55	0.20	0.27	9.31	0.07	0.72	47	8.20	17.47

N is the number of analysis points.

σ is the 1 sigma standard deviation of the measurement.

We declare that we do not have any commercial or associative interest that represents a conflict of interest in connection with the work submitted

Figures

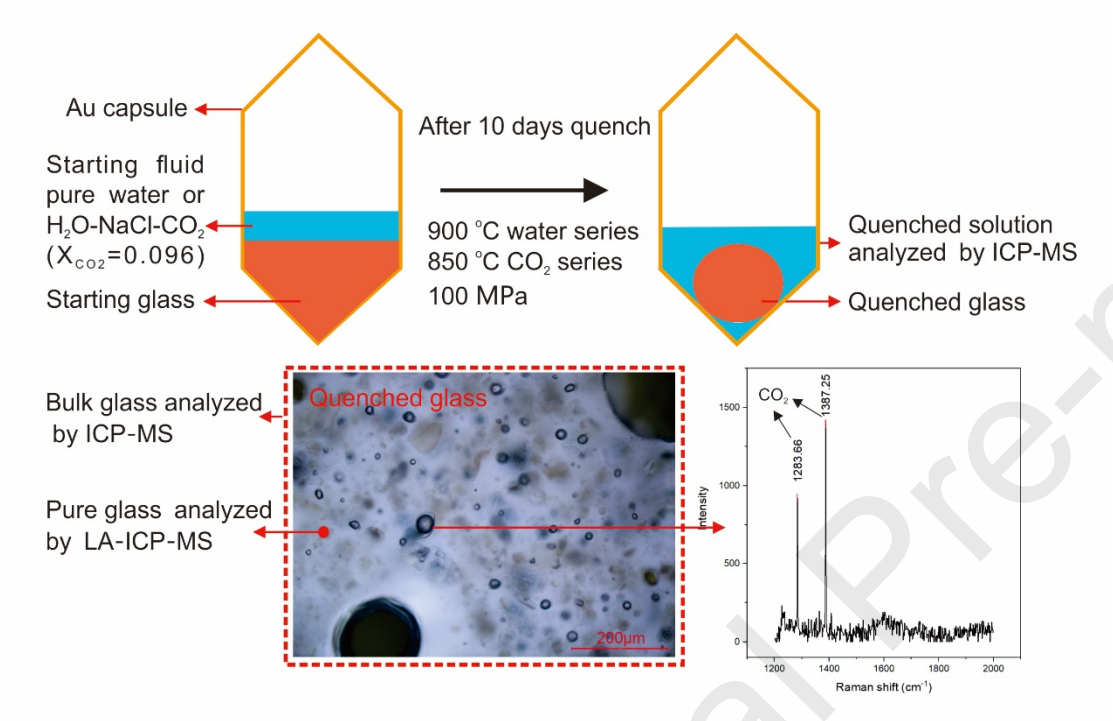

Fig. 1.

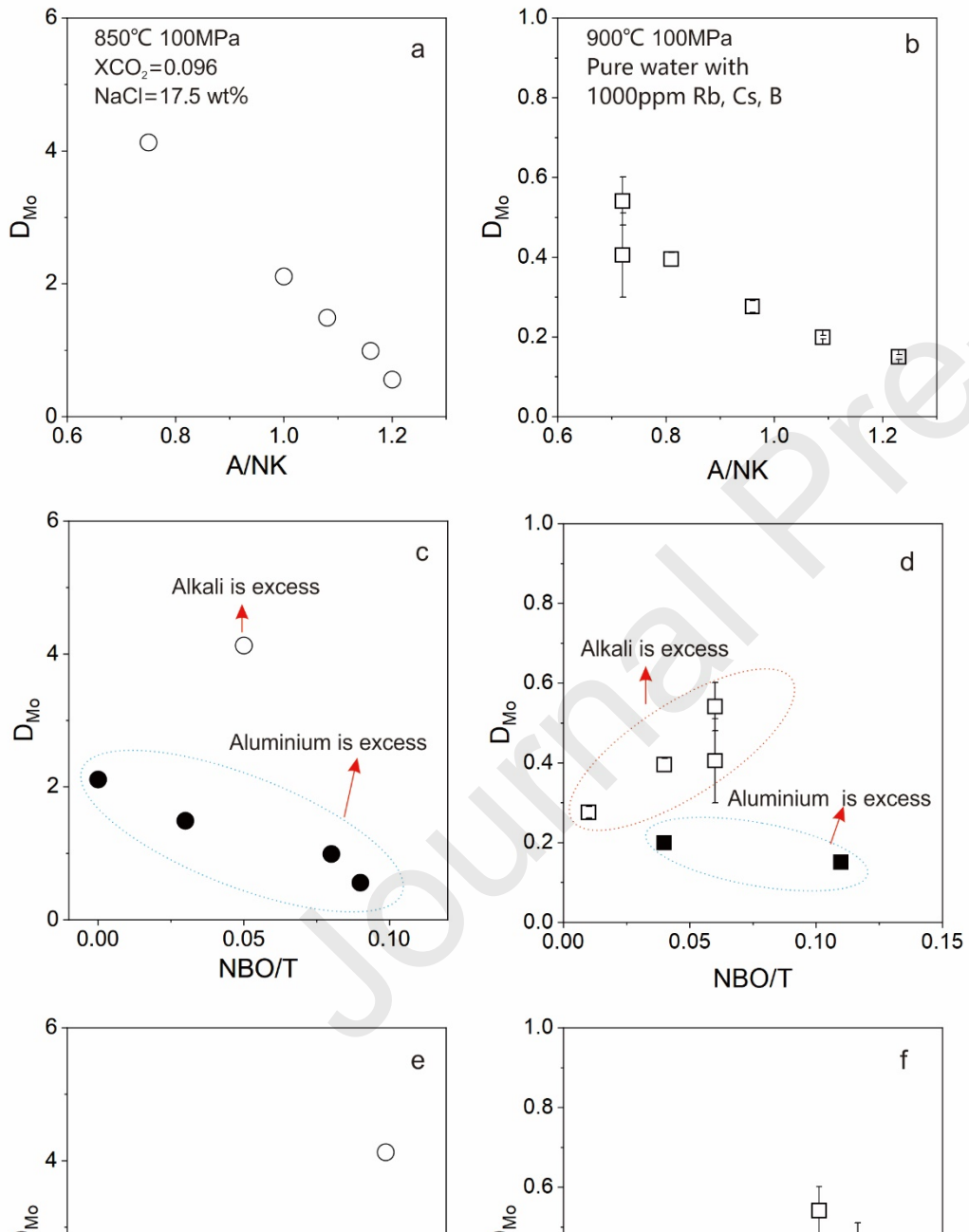

Fig. 2.

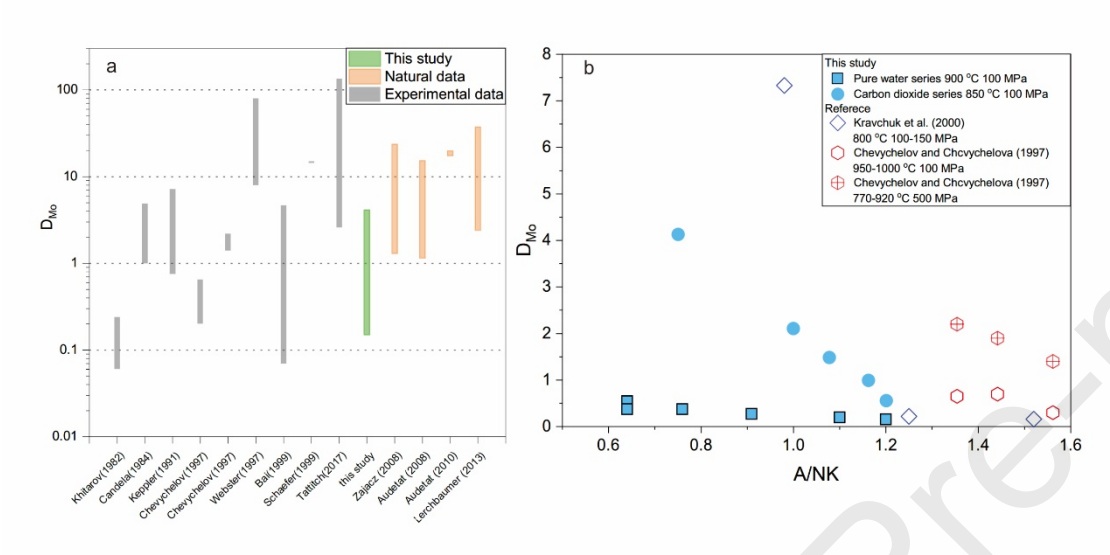

Fig. 3.

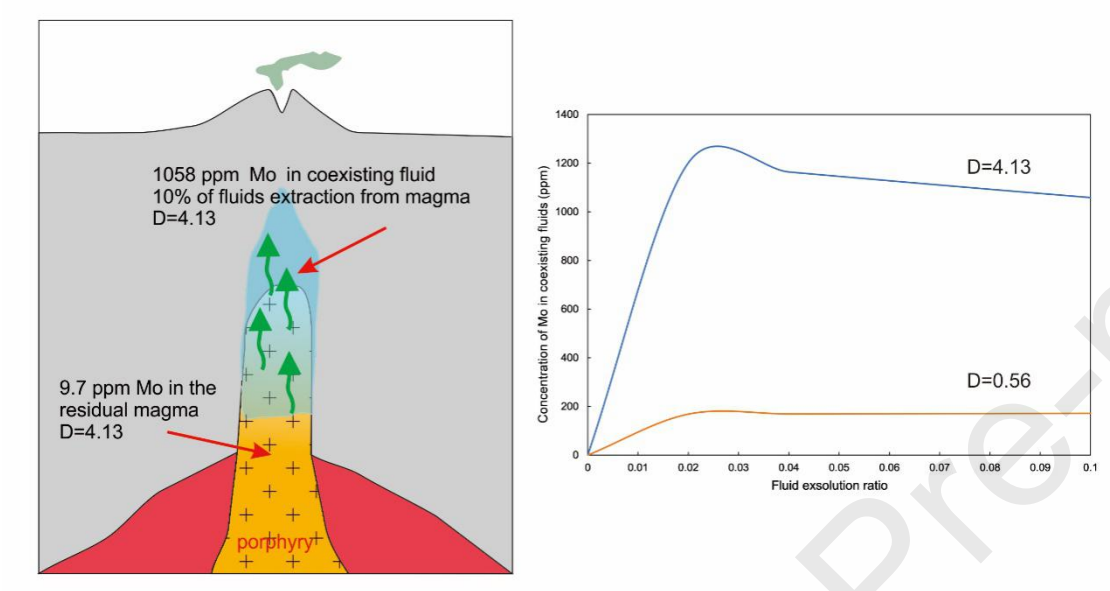

Fig. 4.

Table 1

Starting materials of the three experiments

Run	T °C	P MPa	Na_2O wt.%	Al_2O_3 wt.%	SiO_2 wt.%	K_2O wt.%	A/NK	NBO/T	Mo ppm

The carbon dioxide series (X_{CO_2}= 0.096, 17.5wt.% NaCl)									
M1-1	850	100	5.47	10.86	78.12	5.05	0.75	0.05	952
M1-2	850	100	4.47	12.46	78.20	3.88	1.08	0.03	805
M1-3	850	100	5.12	13.05	76.00	4.27	1.00	0.00	693
M1-4	850	100	4.70	14.42	75.88	3.94	1.20	0.09	717
M1-6	850	100	5.45	15.06	75.70	3.68	1.16	0.08	576
The water series (pure water with 1000ppm Rb, Cs, B)									
J-039	900	100	5.28	11.10	77.12	6.41	0.71	0.06	592
J-040	900	100	5.01	11.86	77.08	5.98	0.81	0.04	497
J-041	900	100	4.23	14.25	76.15	5.30	1.12	0.06	529
J-042	900	100	3.92	12.44	77.59	5.95	0.96	0.01	656
J-043	900	100	3.99	15.26	75.61	5.06	1.27	0.13	591
J-044	900	100	5.28	11.10	77.12	6.41	0.71	0.06	592
The contrast series (11.73 wt.% NaCl, 8.34 wt.% KCl)									
J-003	900	100	4.23	14.25	76.15	5.30	1.12	0.06	529
J-010	900	100	3.99	15.26	75.61	5.06	1.27	0.13	591
J-016	900	100	5.28	11.10	77.12	6.41	0.71	0.06	592

A/NK= $(Al_2O_3)/ (Na_2O + K_2O)$ in mole; $X_{CO_2}= CO_2/ (CO_2 + H_2O)$ in mole; NBO/T is the ratio of non-bridge oxygen to tetrahedron ions, as defined in the discussion section (4.2). The concentrations in parentheses are those of the starting solutions.

Table 2

Compositions of quenched glasses and leaching solution, and the calculated partition coefficient (D_{Mo}) between leaching solution and quenched glasses.

Run.	Na_2O wt.%	Al_2O_3 wt.%	SiO_2 wt.%	K_2O wt.%	A/NK	NBO/T	Mo ppm Quenched solution[a]	Mo ppm Bulk glasses[b]	Mo ppm Pure glasses[c]	σ	D_{Mo} Bulk	D_{Mo} Pure	D_{Mo} σ
The carbon dioxide series													
M1-1	n.a.	n.a.	n.a.	n.a.	0.75	0.05	861	208	n.a.		4.13	n.a.	
M1-2	n.a.	n.a.	n.a.	n.a.	1.08	0.03	539	363	n.a.		1.49	n.a.	
M1-3	n.a.	n.a.	n.a.	n.a.	1.00	0.00	367	174	n.a.		2.11	n.a.	
M1-4	n.a.	n.a.	n.a.	n.a.	1.20	0.09	240	428	n.a.		0.56	n.a.	
M1-6	n.a.	n.a.	n.a.	n.a.	1.16	0.08	353	356	n.a.		0.99	n.a.	
The water series													
J-039	5.40	11.52	75.56	6.65	0.72	0.06	174	n.a.	322	36.0	n.a.	0.54	0.06
J-040	4.78	11.74	76.61	6.12	0.81	0.04	124	n.a.	315	13.0	n.a.	0.39	0.02
J-041	4.11	13.67	76.09	5.36	1.09	0.04	96	n.a.	482	10.8	n.a.	0.20	0.00
J-042	3.76	12.19	77.22	5.98	0.96	0.01	139	n.a.	503	25.7	n.a.	0.28	0.01
J-043	3.89	14.61	75.67	5.01	1.23	0.11	78	n.a.	521	19.5	n.a.	0.15	0.01
J-044	5.63	12.14	74.21	7.03	0.72	0.06	136	n.a.	337	87.8	n.a.	0.40	0.11
The contrast series													
J-003	5.12	14.20	73.96	6.61	0.91	0.02	121	302	351	19.4	0.40	0.34	0.02
J-010	4.51	14.36	74.70	6.28	1.01	0.00	203	437	492	20.3	0.46	0.41	0.02

J-016	6.09	12.08	72.45	9.35	0.60	0.11	238	56	47	8.20	4.23	5.07	0.89

Notes: [a] The concentration of Mo in the fluid phase. All leaching solution was collected and then analyzed using ICP–MS.

[b] The concentration of Mo in quenched glass. The glass was dissolved by HNO_3 and HF and then analyzed using ICP–MS.

[c] The concentration of Mo in quenched glass. LA–ICP–MS was used to avoid analyzing the fluid phase that was trapped in quenched glasses.

σ represents the 1 sigma standard deviation of the measurements.

D_{Mo} bulk means that the partition coefficient was calculated using a/b.

D_{Mo} pure means the partition coefficient was calculated using a/c.

n.a. data were not analyzed.

Table 3

The average composition and the relative standard deviation (RSD) of the quenched glasses of the contrast and water series glasses at randomly different points using LA-ICP-MS.

		Na_2O			Al_2O_3			SiO_2			K_2O			Mo		
	N	wt.%	σ	RSD	wt.%	σ	RSD	wt.%	σ	RSD	wt.%	σ	RSD	ppm	σ	RSD
The water series																
J-039	3	5.40	0.06	1.05	11.52	0.11	0.97	75.56	0.23	0.30	6.65	0.03	0.51	322	36.0	9.93
J-040	7	4.78	0.02	0.50	11.74	0.02	0.20	76.61	0.07	0.10	6.12	0.05	0.80	315	13.0	7.29
J-041	5	4.11	0.10	2.31	13.67	0.29	2.10	76.09	0.45	0.59	5.36	0.07	1.35	482	10.8	2.25
J-042	5	3.76	0.06	1.68	12.19	0.18	1.45	77.22	0.28	0.36	5.98	0.10	1.70	503	25.7	5.10
J-043	5	3.89	0.03	0.84	14.61	0.14	0.99	75.67	0.16	0.21	5.01	0.06	1.11	521	19.5	3.74
J-044	4	5.63	0.08	1.35	12.14	0.82	6.79	74.21	0.99	1.33	7.03	0.19	2.72	337	87.8	3.20
The contrast series																
J-003	6	5.14	0.07	1.32	14.20	0.22	1.58	73.89	0.45	0.60	6.66	0.21	3.09	351	19.4	5.51
J-010	10	4.53	0.08	1.77	14.48	0.24	1.66	74.49	0.37	0.49	6.34	0.15	2.42	492	20.3	4.15
J-016	6	6.10	0.05	0.80	12.01	0.25	2.05	72.55	0.20	0.27	9.31	0.07	0.72	47	8.20	17.47

N is the number of analysis points.

σ is the 1 sigma standard deviation of the measurement.

Highlights

1. In evolved peralkaline residual magma, the molybdenum will easily be distributed into coexisting fluids
2. The distribution coefficient of molybdenum always decreased with increasing A/NK in felsic melts.
3. Compared to the pure water fluids, the distribution coefficient of molybdenum in carbon dioxide bearing salinity fluids is higher.